

SPHERICAL AUTOREGRESSIVE MODELS, WITH APPLICATION TO DISTRIBUTIONAL AND COMPOSITIONAL TIME SERIES

Changbo Zhu and Hans-Georg Müller
Department of Statistics, University of California, Davis
Davis, CA 95616 USA

7 October 2021

ABSTRACT

We introduce a new class of autoregressive models for spherical time series, where the dimension of the spheres on which the observations of the time series are situated may be finite-dimensional or infinite-dimensional as in the case of a general Hilbert sphere. Spherical time series arise in various settings. We focus here on distributional and compositional time series. Applying a square root transformation to the densities of the observations of a distributional time series maps the distributional observations to the Hilbert sphere, equipped with the Fisher-Rao metric. Likewise, applying a square root transformation to the components of the observations of a compositional time series maps the compositional observations to a finite-dimensional sphere, equipped with the geodesic metric on spheres. The challenge in modeling such time series lies in the intrinsic non-linearity of spheres and Hilbert spheres, where conventional arithmetic operations such as addition or scalar multiplication are no longer available. To address this difficulty, we consider rotation operators to map observations on the sphere. Specifically, we introduce a class of skew-symmetric operator such that the associated exponential operators are rotation operators that for each given pair of points on the sphere map one of the points to the other one. We exploit the fact that the space of skew-symmetric operators is Hilbertian to develop autoregressive modeling of geometric differences that correspond to rotations of spherical and distributional time series. Differences expressed in terms of rotations can be taken between the Fréchet mean and the observations or between consecutive observations of the time series. We derive theoretical properties of the ensuing autoregressive models and showcase these approaches with several motivating data. These include a time series of yearly observations of bivariate distributions of the minimum/maximum temperatures for a period of 120 days during each summer for the years 1990-2018 at Los Angeles (LAX) and John F. Kennedy (JFK) international airports. A second data application concerns a compositional time series with annual observations of compositions of energy sources for power generation in the U.S..

KEY WORDS: Distributional Data, Compositional Data, Hilbert Sphere, Fisher-Rao Metric, Geodesics, Skew-Symmetric Operators, Rotation Operators, Random Objects.

1. Introduction

Modern day data analysts increasingly encounter complex data types where data are no longer traditional vectors, and furthermore are not situated in a linear space such as a Hilbert space. Such non-Euclidean data may also be encountered in the form of a time series. At this point, the methodology available for the analysis of such data is quite limited. An exception are recent efforts to develop models for distributional time series in the context of the rapidly evolving field of distributional data analysis (DDA) (Petersen et al. 2021). A simple approach for distributional time series is to represent distributions by square integrable functions via the log quantile density transformation or a similar transformation (Petersen and Müller 2016); a downside is that such transformations may lead to large metric distortions. The distributional time series is then transformed to a functional time series, which have been well investigated (Bosq 2000). Geometric approaches that are based on constructing tangent bundles on the Wasserstein manifold have recently been shown to provide better predictions for autoregressive models (Chen et al. 2021; Zhang et al. 2021), while an autoregressive model that is intrinsic to the Wasserstein manifold can be based on a recently developed transport algebra (Zhu and Müller 2021). It bears emphasizing that all these methods are limited to the case of distributional time series composed of one-dimensional distributions.

Modeling distributional time series has been limited to the case of sequences of one-dimensional distributions, as the challenges of characterizing optimal transport as well as the Wasserstein manifold and its parallel transport for the case of multivariate distributions are formidable, in addition to numerical difficulties, and viable transformations have not yet been developed. For both multivariate and one-dimensional distributions the Fisher-Rao metric provides an alternative to the popular Wasserstein metric that is easily to work with both numerically and theoretically, irrespective of the dimension of the distributions. This distributional metric is characterized by its invariance under diffeomorphisms and the ease of explicitly computing geodesics in the space of distributions with smooth densities equipped with this metric (Friedrich 1991; Bauer et al. 2016). Of special interest for statistical applications is that the Fisher-Rao metric can be easily extended to multivariate distributions, and neither analysis

nor numerical implementations face difficulties in the multivariate case, and the geodesics in distribution space are always well-defined irrespective of the dimension.

We focus here on time series data with observations that reside naturally or can be equivalently represented as points on a sphere $\mathcal{S} = \{x \in \mathcal{H} : \|x\|_{\mathcal{H}} = 1\}$, where \mathcal{H} is a real separable Hilbert space with inner product $\langle \cdot, \cdot \rangle_{\mathcal{H}}$ and norm $\|x\|_{\mathcal{H}} := \sqrt{\langle x, x \rangle_{\mathcal{H}}}$. The sphere \mathcal{S} can be finite-dimensional in which case we denote it by \mathcal{S}^d if $\mathcal{H} = \mathbb{R}^{d+1}$ or infinite-dimensional when $\mathcal{H} = L^2$ or any isomorphic space and in this case we refer to it as the Hilbert sphere and denote it by \mathcal{S}^{∞} . Our focus on spherical time series is motivated by the convenience of incorporating different data types such as compositional data, directional data and distributional data.

Compositional data take values in the simplex

$$\mathcal{C}^d = \left\{ \mathbf{z} = (z_1, z_2, \dots, z_d)^T \in \mathbb{R}^d \mid z_i \geq 0 \text{ for all } i = 1, 2, \dots, d \text{ and } \sum_{i=1}^d z_i = \kappa \right\},$$

where $\kappa > 0$ is a constant with default value $\kappa = 1$, in which case these data are non-negative proportions that sum to 1. By applying the point-wise square root ratio (psr) transformation $\text{psr} : \mathcal{C}^d \rightarrow \mathcal{S}^{d-1}$, defined as

$$\text{psr}(\mathbf{z}) = \left(\sqrt{z_1/\kappa}, \sqrt{z_2/\kappa}, \dots, \sqrt{z_d/\kappa} \right)^T, \quad (1)$$

\mathcal{C}^d can be mapped into a subset of \mathcal{S}^{d-1} . This maps compositional time series to finite-dimensional spherical time series (Scealy and Welsh 2011; Dai and Müller 2018). Examples of compositional time series are common and include for example repeated election cycles when there are several parties and the compositions correspond to the vote shares of each party; or color preferences of car buyers that change from year to year, reflected in the percentage of cars sold in a specific color. In section 5.2, we illustrate the proposed spherical autoregressive models (SAR) with compositional time series that correspond to the annually recorded proportions of electricity generated from different energy sources in the U.S., where energy sources include coal, natural gas or nuclear and renewable sources. The composition of energy sources has a major

impact on the carbon dioxide (CO₂) emissions that accrue from electricity generation over time.

Data that can be represented by locations on finite-dimensional spheres are ubiquitous and are not limited to compositional data but also include directional data such as wind directions. For example, the study of ocean surface wind over time is important in determining the spread of aerial organisms (Felicísimo et al. 2008). Sequences of hourly or daily recorded wind directions are naturally represented as a spherical time series with observations in \mathcal{S}^2 . Another application of \mathcal{S}^d -valued time series are vector time series, where the vector observations can be expressed in polar coordinates and then form a spherical time series and a scalar time series where the latter corresponds to the length of the vector at time t . In some cases the length of the vector may not be relevant if one is primarily interested in the association between the vector components as reflected by the direction of the vector. Then only the sequence of directions of the vector components matters and if the original vector data have dimension $d + 1$, the directions are represented on \mathcal{S}^d and again one has a spherical time series.

For any density function $f : \mathbb{R}^D \rightarrow \mathbb{R}$, where f satisfies $f \geq 0$ and $\int_{\mathbb{R}^D} f(x)dx = 1$, we define the functional point-wise square root transformation (fpsr) as

$$\text{fpsr}(f) = g, \text{ where } g(\mathbf{z}) = \sqrt{f(\mathbf{z})} \text{ for all } \mathbf{z} \in \mathbb{R}^D.$$

Using fpsr, distributional data correspond to the elements of a segment of the Hilbert sphere \mathcal{S}^∞ equipped with the Fisher-Rao metric (Dai 2022) and distributional time series then are accordingly represented as \mathcal{S}^∞ -valued time series. For two-dimensional distributions, of daily maximum and minimum temperatures recorded for 24 hours over the summer months at airports in the U.S. Considering these two-dimensional distributions over successive years then forms a time series with \mathcal{S}^∞ -valued observations. These time series are of interest for assessing the effects of climate change and the risks and costs associated with rising temperatures.

Time series analysis for Euclidean vector data is a well-established field and both parametric and non-parametric methods have been developed. (Fan and Yao 2017, 2003). For functional or Hilbert-space valued time series linear and autoregressive process models have also been well

studied, starting with Bosq (2000). In contrast to these developments, there is so far very little work on time series with random objects, i.e., random variables in general metric spaces (Müller 2016). Even for the special case of spherical time series the literature is scarce. An interesting approach is spherical regression for the non-time series case when one has i.i.d. data with predictors and responses located in $\mathcal{S} = \mathcal{S}^d$ (Chang 1986, 1989; Kim 1998; Marzio et al. 2019), where the key ingredient is a rotation matrix in the set of orthogonal matrices $\text{SO}(d+1)$ that rotates the predictor to the response. In addition, Downs (2003) and Rosenthal et al. (2014) introduced some more general families of transformations and Shi et al. (2021) investigated settings where predictors and responses might have mismatches. However, all these methods are established under the i.i.d. regression setting and limited to the finite-dimensional case ($d < \infty$); furthermore, they accommodate only one predictor, while for autoregressive modeling one needs to accommodate the joint action of predictors from multiple lags.

The main challenge of modeling time series in non-linear spaces such as \mathcal{S} is that conventional operations like addition and subtraction are not available. This lack of algebraic operations imposes a fundamental limitation for autoregressive modeling. To overcome the challenge of non-linearity for the case of spherical time series, we utilize the geometric structure of \mathcal{S} . The geodesic distance on \mathcal{S} is defined as $d(x_1, x_2) = \arccos(\langle x_1, x_2 \rangle)$ for any $x_1, x_2 \in \mathcal{S}$. Geodesics are locally length-minimizing paths between points that are well-defined in geodesic metric spaces, where the length of a geodesic path between two points coincides with the distance of the points (Burago et al. 2001). The geodesics of spheres correspond to great circles. The key idea for the modeling of spherical autoregressive (SAR) time series is that the geodesic between two points $x_1, x_2 \in \mathcal{S}$ can be written as $\gamma(a) = \exp(aL)$, where $a \in [0, 1]$ and $L : \mathcal{H} \rightarrow \mathcal{H}$ is a skew-symmetric operator. We then relate the spherical difference between x_1 and x_2 to the operator L , which is a linear operator. This makes it possible to model the differenced times series in the linear space of skew-symmetric operators.

We study two versions of autoregressive models for spherical time series. In the basic SAR model the autoregressive model is based on the spherical equivalent of differences between the observations and the overall Fréchet mean as arguments. A second model, referred to as DSAR, is

based on the spherical differences between consecutive observations. These models can be applied for autoregressive modeling on spheres \mathcal{S} of finite or infinite dimension and their implementation is computationally efficient.

The rest of the paper is organized as follows. In Section 2, we introduce the rotation and log rotation operators in Hilbert spaces and present a key relationship between rotations and skew-symmetric operators. Methodology and theory are in Section 3, which contains the main results. Estimation and prediction are studied in Section 4. We report results for data applications to distributional and compositional time series in Section 5, which is followed by a discussion section in Section 6.

2. Rotations and Skew-Symmetric Operators

Let \mathcal{H} be a real separable Hilbert space with inner product $\langle \cdot, \cdot \rangle_{\mathcal{H}}$ and norm $\|x\|_{\mathcal{H}} := \sqrt{\langle x, x \rangle_{\mathcal{H}}}$. The Hilbert sphere \mathcal{S} is a subset of \mathcal{H} whose elements have norm 1, i.e., $\mathcal{S} = \{x \in \mathcal{H} : \|x\|_{\mathcal{H}} = 1\}$. Given a set of points $\{x_1, x_2, \dots, x_m\} \subset \mathcal{S}$, let $\text{span}\{x_1, x_2, \dots, x_m\} = \{a_1x_1 + a_2x_2 + \dots + a_mx_m : a_1, a_2, \dots, a_m \in \mathbb{R}\} \subset \mathcal{H}$ denote the m -dimensional subspace of \mathcal{H} spanned by x_1, x_2, \dots, x_m . The set of bounded linear operators on \mathcal{H} is denoted as $\mathcal{B}(\mathcal{H})$ and an operator $Q \in \mathcal{B}(\mathcal{H})$ is skew-symmetric if

$$\langle Qx, y \rangle + \langle x, Qy \rangle = 0 \text{ for all } x, y \in \mathcal{H}.$$

For any bounded linear operator $L : \mathcal{H} \rightarrow \mathcal{H}$, define its exponential as $\exp(L) := \sum_{l=0}^{\infty} L^l / l!$. An orthogonal operator $O \in \mathcal{B}(\mathcal{H})$ is a rotation operator if and only if there exists a skew-symmetric operator Q such that $O = \exp(Q)$ (Martin 1932).

For each skew-symmetric operator Q there is a unique rotation operator $\exp(Q)$. Let $\mathcal{R}(\mathcal{H})$ and $\mathcal{S}(\mathcal{H})$ be the set of rotation operators and skew-symmetric operators respectively, then by definition $\mathcal{R}(\mathcal{H}) = \exp(\mathcal{S}(\mathcal{H}))$. If $\{e_1, e_2, \dots\}$ is an orthonormal basis of \mathcal{H} , then $\mathcal{S}(\mathcal{H})$ admit

the following orthonormal basis

$$\mathcal{S}(\mathcal{H}) = \text{span} \{e_i \otimes e_j - e_j \otimes e_i : i, j = 1, 2, \dots\} \subset \mathcal{H} \otimes \mathcal{H},$$

where $\mathcal{H} \otimes \mathcal{H}$ is the tensor product of the Hilbert space \mathcal{H} with itself and is also a Hilbert space with inner product

$$\langle x_1 \otimes y_1, x_2 \otimes y_2 \rangle_{\mathcal{H} \otimes \mathcal{H}} = \langle x_1, x_2 \rangle_{\mathcal{H}} \langle y_1, y_2 \rangle_{\mathcal{H}},$$

with $x_1, x_2, y_1, y_2 \in \mathcal{H}$; the inner product $\langle \cdot, \cdot \rangle_{\mathcal{H} \otimes \mathcal{H}}$ can be extended to any element in $\mathcal{H} \otimes \mathcal{H}$ by linearity. Observing that $\mathcal{S}(\mathcal{H})$ is a closed subspace of $\mathcal{H} \otimes \mathcal{H}$ with respect to $\langle \cdot, \cdot \rangle_{\mathcal{H} \otimes \mathcal{H}}$, $\mathcal{S}(\mathcal{H})$ is seen to be a complete separable Hilbert space.

Given two points $x_1, x_2 \in \mathcal{H}$ such that $x_1 \neq x_2$ and $x_1 \neq -x_2$, the proposed methodology relies on rotation operators that provide a rotation on \mathcal{S} within the two dimensional subspace $\text{span}\{x_1, x_2\}$.

Theorem 1. *Set $u_1 = x_1$ and $u_2 = (x_2 - \langle x_2, u_1 \rangle u_1) / \|x_2 - \langle x_2, u_1 \rangle u_1\|_{\mathcal{H}}$. Let I be the identity operator and $Q := u_1 \otimes u_2 - u_2 \otimes u_1 \in \mathcal{S}(\mathcal{H})$. Then, given an angle $\vartheta \in [0, 2\pi]$,*

$$\exp(\vartheta Q) = I + \sin(\vartheta)Q + (1 - \cos(\vartheta))Q^2 \tag{2}$$

is a rotation operator that rotates counterclockwise within $\text{span}\{u_1, u_2\}$ by ϑ , i.e.,

- *For any $y_1, y_2 \in \mathcal{H}$, $\langle \exp(\vartheta Q)y_1, \exp(\vartheta Q)y_2 \rangle_{\mathcal{H}} = \langle y_1, y_2 \rangle_{\mathcal{H}}$.*
- *For any $x \in \text{span}\{u_1, u_2\} \cap \mathcal{S}$, $\arccos \langle \exp(\vartheta Q)x, x \rangle_{\mathcal{H}} = \vartheta$.*
- *For any $y \in \mathcal{H}$ perpendicular to $\text{span}\{u_1, u_2\}$, i.e., $\langle y, u_1 \rangle_{\mathcal{H}} = 0$ and $\langle y, u_2 \rangle_{\mathcal{H}} = 0$, it holds that $\exp(\vartheta Q)y = y$.*

For $\mathcal{H} = \mathbb{R}^3$, Figure 1 provides an illustration of the rotation operator $\exp(\vartheta Q)$. We note that (2) reduces to the Rodrigues rotation formula in this special case. For a rotation operator

$\exp(\vartheta L)$ in higher dimensional Hilbert spaces such as \mathbb{R}^d with $d > 3$, where L is an arbitrary skew-symmetric operator, the equality $\exp(\vartheta L) = I + \sin(\vartheta)L + (1 - \cos(\vartheta))L^2$ will not hold in general. That (2) is satisfied for any separable space \mathcal{H} is due to the fact that $\exp(\vartheta Q)$ is a special rotation that only rotates within the two-dimensional subspace $\text{span}\{u_1, u_2\}$.

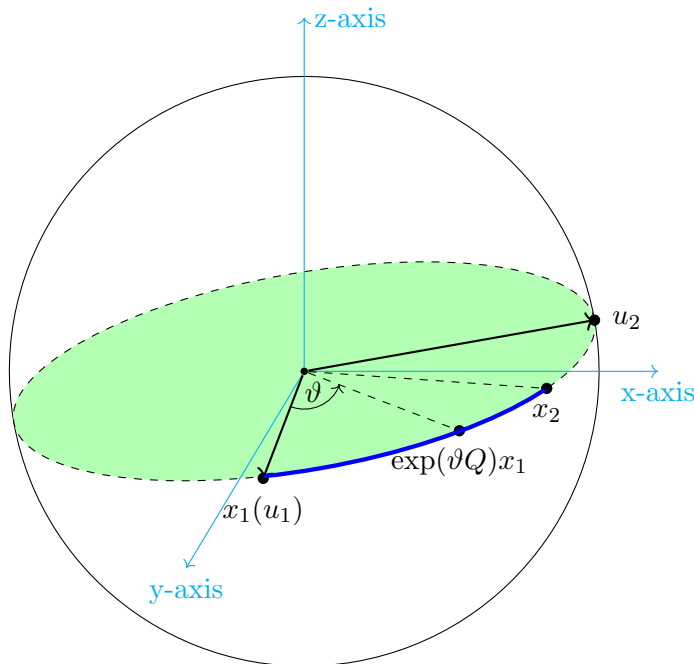


Figure 1: Illustration of the rotation operator $\exp(\vartheta Q)$ when $\mathcal{H} = \mathbb{R}^3$. The green plane is the two-dimensional subspace spanned by u_1 and u_2 . By construction, u_1, u_2 are orthogonal and the angle between them is $\pi/2$. Here $\exp(\vartheta Q)x_1$ is the location of the image of the rotation operator $\exp(\vartheta Q)$ applied at x_1 and ϑ is the angle between x_1 and $\exp(\vartheta Q)x_1$. The blue line is the geodesic between x_1 and x_2 that is traced by the path $\gamma(a) := \exp(a\theta Q)x_1$, where $a \in [0, 1]$ and $\theta = \arccos(\langle x_1, x_2 \rangle)$. It can be easily seen that $\gamma(0) = x_1$ and $\gamma(1) = x_2$.

3. Spherical Autoregressive Models

Based on the rotation operator introduced earlier, the geodesic $\gamma : [0, 1] \rightarrow \mathcal{S}$ between two points $x_1, x_2 \in \mathcal{S}$ can be traced by rotating x_1 to x_2 within the two dimensional subspace spanned by $\{x_1, x_2\}$ around the origin, i.e.,

$$\gamma(a) = \exp(a\theta Q)x_1.$$

where $a \in [0, 1]$, $\theta = \arccos(\langle x_1, x_2 \rangle)$ is the angle between x_1 and x_2 and Q is the same as in Theorem 1; see Figure 1 for a demonstration of $\gamma(a)$ when $\mathcal{H} = \mathbb{R}^3$. We then utilize geodesics on \mathcal{S} to arrive at a notion of difference between points on \mathcal{S} . Starting with the Euclidean space \mathbb{R}^d and considering two elements $w_1, w_2 \in \mathbb{R}^d$, the difference $V = w_2 - w_1$ can be interpreted as the optimal transport map that moves w_1 to w_2 and the geodesic between them is the straight line $r(a) = w_1 + aV$ where $a \in [0, 1]$; see Zhu and Müller (2021) for a similar extension of this idea to the Wasserstein space. On the other hand, not only $\exp(\theta Q)$ may be interpreted as the optimal transport map that moves x_1 to x_2 but also the geodesic can be constructed based on $\exp(\theta Q)$. This motivates us to define the spherical difference between points x_1 and x_2 on \mathcal{S} ,

$$x_2 \ominus x_1 := \theta Q.$$

Given a sequence of data points $x_1, x_2, \dots, x_n \in \mathcal{S}$ with the same Fréchet mean μ_x , i.e., $\mu_x := \operatorname{argmin}_{z \in \mathcal{S}} \mathbb{E}[d_{\mathcal{S}}^2(z, x_t)]$ for all $t = 1, 2, \dots, n$, we then construct a new series by taking differences between the x_t and the Fréchet mean μ_x ,

$$\{R_t := x_t \ominus \mu_x : t = 1, 2, \dots, n\} \subset \mathcal{S}(\mathcal{H}).$$

Assuming that $\{R_t\}$ is a stationary sequence (Bosq 2000), we propose the following spherical autoregressive (SAR) model of order p ,

$$R_t - \mu_R = \alpha_1(R_{t-1} - \mu_R) + \dots + \alpha_p(R_{t-p} - \mu_R) + \varepsilon_t \text{ where } R_t = x_t \ominus \mu_x, \quad (3)$$

where $\alpha_1, \dots, \alpha_p \in \mathbb{R}$, $\mu_R = E[R_t]$ and $\{\varepsilon_t\} \subset \mathcal{S}(\mathcal{H})$ are i.i.d random innovations with mean 0.

To elucidate the connection of this model with the previously studied spherical regression (Chang 1986, 1989; Kim 1998; Marzio et al. 2019), which has not yet been extended to a time series framework and admits only one predictor, consider a regression setting with x_t as single predictor and y_t as response. In the above difference notation, this previously studied spherical regression can be written as $y_t \ominus x_t = R_0 + \varepsilon_t$. In the Euclidean space \mathbb{R}^d this corresponds to an

intercept only regression model $z_t - w_t = \beta_0 + \epsilon_t$, where $z_t \in \mathbb{R}^d$ is the response, $w_t \in \mathbb{R}^d$ is the predictor, $\beta_0 \in \mathbb{R}^d$ is the intercept and $\{\epsilon_t\} \subset \mathbb{R}^d$ are i.i.d. errors. By taking expectation on both sides, we observe that $E[z_t] - E[w_t] = \beta_0$. In some sense, this corresponds to a special case of Model (3) where $p = 1$ and the single “slope” is $\alpha_1 = 1$ as then one obtains $y_t \ominus \mu_y = x_t \ominus \mu_x + \epsilon_t$ and its Euclidean counterpart $z_t - E[z_t] = w_t - E[w_t] + \epsilon_t$, which is equivalent to $z_t - w_t = \beta_0 + \epsilon_t$.

As alternative to the SAR model (3) we also consider a second model that is based on the spherical differences of consecutive observations. This difference based spherical autoregressive model (DSAR) is given by

$$R_t - \mu_R = \alpha_1(R_{t-1} - \mu_R) + \cdots + \alpha_p(R_{t-p} - \mu_R) + \varepsilon_t, \text{ where } R_t = x_{t+1} \ominus x_t, \quad (4)$$

where as before, $\alpha_1, \dots, \alpha_p \in \mathbb{R}$, $\mu_R = E[R_t]$ and $\{\varepsilon_t\} \subset \mathcal{S}(\mathcal{H})$ are i.i.d random innovations with mean 0.

Differencing is an inherent feature of DSAR models and is a common technique to reduce trend and seasonality for time series in Euclidean space. It may also be useful for some spherical time series. For example, the US energy mix compositional time series, which we will discuss further in Section 5.2, shows a trend over the years, as more clean energy is generated each year and coal/petroleum fuels are increasingly phased out.

Regarding the existence of stationary solutions of the proposed SAR model, the following result is a consequence of Theorem 3.3 of Zhang et al. (2021).

Theorem 2. *Assuming that $\{R_t : t \in \mathbb{N}\}$ is stationary, $E\langle \varepsilon_t, \varepsilon_t \rangle_{\mathcal{H} \otimes \mathcal{H}} < \infty$ and the roots of $\phi(z) = 1 - \alpha_1 z - \cdots - \alpha_p z^p$ are outside the unit circle, then*

$$R_t - \mu_R = \sum_{i=0}^{\infty} \psi_i \varepsilon_{t-i}$$

is a unique stationary solution of

$$R_t - \mu_R = \alpha_1(R_{t-1} - \mu_R) + \cdots + \alpha_p(R_{t-p} - \mu_R) + \varepsilon_t, \quad t \in \mathbb{N},$$

where $\{\psi_t\}$ is absolutely summable and determined by $1/\phi(z) = \sum_{i=0}^{\infty} \psi_i z^i$.

4. Estimation and Prediction

4.1 Estimation

We use Yule-Walker type estimators for the estimation of the coefficients $\alpha_1, \alpha_2, \dots, \alpha_p$ of the SAR and DSAR models. Setting

$$\lambda_k = E[\langle R_1 - \mu_R, R_{k+1} - \mu_R \rangle_{\mathcal{H} \otimes \mathcal{H}}],$$

it is straight-forward to check that the model parameters satisfy

$$\begin{pmatrix} \lambda_1 \\ \lambda_2 \\ \vdots \\ \lambda_p \end{pmatrix} = \begin{pmatrix} \lambda_0 & \lambda_1 & \cdots & \lambda_{p-1} \\ \lambda_1 & \lambda_0 & \cdots & \lambda_{p-2} \\ \vdots & \vdots & & \vdots \\ \lambda_{p-1} & \lambda_{p-2} & \cdots & \lambda_0 \end{pmatrix} \begin{pmatrix} \alpha_1 \\ \alpha_2 \\ \vdots \\ \alpha_p \end{pmatrix}.$$

Replacing λ_k by sample estimates

$$\hat{\lambda}_k = \frac{1}{n-k} \sum_{t=1}^{n-k} \langle R_t - \hat{\mu}_R, R_{t+k} - \hat{\mu}_R \rangle_{\mathcal{H} \otimes \mathcal{H}}, \quad \hat{\mu}_R = \frac{1}{n} \sum_{t=1}^n R_t \quad (5)$$

then suggests the following estimates $\hat{\alpha}_1, \dots, \hat{\alpha}_p$ for the model parameters $\alpha_1, \dots, \alpha_p$,

$$\begin{pmatrix} \hat{\alpha}_1 \\ \hat{\alpha}_2 \\ \vdots \\ \hat{\alpha}_p \end{pmatrix} = \begin{pmatrix} \hat{\lambda}_0 & \hat{\lambda}_1 & \cdots & \hat{\lambda}_{p-1} \\ \hat{\lambda}_1 & \hat{\lambda}_0 & \cdots & \hat{\lambda}_{p-2} \\ \vdots & \vdots & & \vdots \\ \hat{\lambda}_{p-1} & \hat{\lambda}_{p-2} & \cdots & \hat{\lambda}_0 \end{pmatrix}^{-1} \begin{pmatrix} \hat{\lambda}_1 \\ \hat{\lambda}_2 \\ \vdots \\ \hat{\lambda}_p \end{pmatrix}. \quad (6)$$

Writing $\boldsymbol{\lambda} = (\lambda_0, \lambda_1, \dots, \lambda_p)^T$ and $\hat{\boldsymbol{\lambda}} = (\hat{\lambda}_0, \hat{\lambda}_1, \dots, \hat{\lambda}_p)^T$, we next establish asymptotic normality for $\hat{\boldsymbol{\lambda}}$.

Theorem 3. *Under the assumptions of Theorem 2, it holds that*

$$\sqrt{n}(\widehat{\boldsymbol{\lambda}} - \boldsymbol{\lambda}) \rightarrow^d N(0, V), \quad V = \left(\sum_{h=-\infty}^{\infty} \Gamma_{u,v}^h \right)_{u,v=0,1,\dots,p},$$

where, setting $\kappa(u) = \sum_{i=-\infty}^{\infty} \psi_i \psi_{i+u}$,

$$\begin{aligned} \Gamma_{u,v}^h &= (E[\langle \varepsilon_1, \varepsilon_1 \rangle^2] - (E[\langle \varepsilon_1, \varepsilon_1 \rangle])^2 - 2E[\langle \varepsilon_1, \varepsilon_2 \rangle^2]) \sum_{i=-\infty}^{\infty} \psi_i \psi_{i+u} \psi_{i+h} \psi_{i+h+v} \\ &\quad + (E[\langle \varepsilon_1, \varepsilon_1 \rangle])^2 \kappa(u) \kappa(v) + E[\langle \varepsilon_1, \varepsilon_2 \rangle^2] (\kappa(h) \kappa(h+v-u) + \kappa(h+v) \kappa(h-u)). \end{aligned}$$

For the case where $\{\varepsilon_t\}$ are i.i.d random innovations in \mathbb{R} , the $\Gamma_{u,v}^h$ are identical to those in Bartlett's formula. To show the convergence of $\widehat{\alpha}_1, \dots, \widehat{\alpha}_p$, we set

$$\Lambda = \begin{pmatrix} \lambda_0 & \lambda_1 & \cdots & \lambda_{p-1} \\ \lambda_1 & \lambda_0 & \cdots & \lambda_{p-2} \\ \vdots & \vdots & & \vdots \\ \lambda_{p-1} & \lambda_{p-2} & \cdots & \lambda_0 \end{pmatrix} \text{ and } \widehat{\Lambda} = \begin{pmatrix} \widehat{\lambda}_0 & \widehat{\lambda}_1 & \cdots & \widehat{\lambda}_{p-1} \\ \widehat{\lambda}_1 & \widehat{\lambda}_0 & \cdots & \widehat{\lambda}_{p-2} \\ \vdots & \vdots & & \vdots \\ \widehat{\lambda}_{p-1} & \widehat{\lambda}_{p-2} & \cdots & \widehat{\lambda}_0 \end{pmatrix}.$$

Suppose that $\det(\Lambda) \neq 0$, it then follows from the continuous mapping theorem that $\widehat{\Lambda}^{-1} \rightarrow^p \Lambda^{-1}$ and thus by Theorem 3, we have

Corollary 1. *Under the assumptions of Theorem 2, if $\det(\Lambda) \neq 0$,*

$$\sqrt{n} \left(\begin{pmatrix} \widehat{\alpha}_1 \\ \vdots \\ \widehat{\alpha}_p \end{pmatrix} - \begin{pmatrix} \alpha_1 \\ \vdots \\ \alpha_p \end{pmatrix} \right) \rightarrow^d N \left(0, \Lambda \widetilde{V} (\Lambda^T)^{-1} \right), \text{ where } \widetilde{V} = \left(\sum_{h=-\infty}^{\infty} \Gamma_{u,v}^h \right)_{u,v=1,\dots,p}.$$

We note that in applications involving distributional time series the distributions and specifically the density functions f_t are usually not directly observed and must be inferred from available samples of size N_t , $\{z_{i,t} \in \mathbb{R}^D : i = 1, 2, \dots, N_t\} \sim^{i.i.d} f_t$ that they generate. The random

mechanism that generates the samples is assumed to be independent from the mechanism that generates the random distributions.

To assess the impact of this preliminary estimation step, we provide one requires additional assumptions as follows: All densities f_t have the same compact domain $A \subset \mathbb{R}^D$ and are continuously differentiable on their support; there is a sequence $N \rightarrow \infty$ such that $N_t \geq N$ for all t ; there exists a constant M such that for all t , $\sup_{a \in A} |f_t(a)|$, $\sup_{a \in A} 1/|f_t(a)|$, $\sup_{a \in A} \|f'_t(a)\|$ are all bounded by M , where $\|f'_t(a)\|$ is the norm of the gradient vector. Extending the arguments and construction in Petersen and Müller (2016) to the case of multivariate distributions leads to density estimators \hat{f}_t that satisfy

$$\sup_t P \left(\sup_{a \in A} \left| \hat{f}_t(a) - f_t(a) \right| > c_1 N^{-c_2} \right) \rightarrow 0$$

for constants $c_1, c_2 > 0$, where c_2 depends on the dimension of the distributions and decreases when the dimension increases. One can then show that substituting \hat{f}_t for f_t in R_t in models (3) and (4) and choosing the sample size $N = N(n)$ available for the estimation of each density f_t such that $N^{-c} = o_p(n^{-1/2})$ implies that Theorem 3 and Corollary 1 still hold when using estimated instead of true densities in the fitting of the SAR models under these additional assumptions.

4.2 Prediction

With estimates $\hat{\alpha}_1, \dots, \hat{\alpha}_p$ based on data sequence $\{R_1, \dots, R_n\}$ in hand, the prediction for the skew-symmetric operator at time $n + 1$ is

$$\hat{R}_{n+1} = \hat{\mu}_R + \hat{\alpha}_1(R_n - \hat{\mu}_R) + \dots + \hat{\alpha}_p(R_{n-p+1} - \hat{\mu}_R),$$

with a slight abuse of notation, as in model DSAR, the sequence of observations available for the prediction is of length $n + 1$, i.e., $\{x_i : i = 1, 2, \dots, n + 1\}$, whereas in model SAR it is of length n . Once \hat{R}_{n+1} has been obtained, the prediction of the next observation in the original time series is $\hat{x}_{n+1} := \exp(\hat{R}_{n+1})\mu_x$ when modeling with SAR and $\hat{x}_{n+2} := \exp(\hat{R}_{n+1})x_{n+1}$ for

DSAR.

For a distributional time series of D -dimensional distributions (or density functions), we set $\mathcal{H} = \{f : \mathbb{R}^D \rightarrow \mathbb{R} \mid \int_{\mathbb{R}^D} f^2(a) da < \infty\}$ with inner product $\langle f, g \rangle_{\mathcal{H}} = \int_{\mathbb{R}^D} f(a)g(a) da$ and require the predictions to be constrained in the positive orthant $\mathcal{H}_+ := \{f \in \mathcal{H} : f(a) \geq 0 \text{ for all } a \in \mathbb{R}^D\}$. Similarly, for compositional time series, $\mathcal{H} = \mathbb{R}^d$ and the prediction is constrained to lie in $\mathcal{H}_+ = \{\mathbf{z} = (z_1, \dots, z_d)^T \in \mathbb{R}^d : z_i \geq 0 \text{ for all } i\}$. Writing $x_{\text{rot}} = \exp(Q)x$ for the rotation $\exp(Q)$ of $x \in \mathcal{H}_+$, we use projection operators to enforce the constraint; see Chen et al. (2021) and Pegoraro and Beraha (2021) for related projections in Wasserstein space.

A first option is to use a projection operator Proj^1 to rotate x_{rot} back to the boundary of \mathcal{H}_+ , i.e., $\text{Proj}^1(x_{\text{rot}}) := \exp(c_1 Q)x$, where $c_1 = \sup\{c : c \in [0, 1] \text{ and } \exp(cQ)x \in \mathcal{H}_+\}$. A second option is the operator Proj^2 to project x_{rot} to the nearest point in \mathcal{H}_+ , i.e., $\text{Proj}^2(x_{\text{rot}}) = \text{argmin}_{y \in \mathcal{H}_+} \langle x_{\text{rot}} - y, x_{\text{rot}} - y \rangle$; see Figure 2 for a schematic illustration. We note that Proj^1 may be more useful for SAR, as all the predictions are based on rotations from the Fréchet mean, which may be more likely to stay away from the boundary of \mathcal{H}_+ under stationarity assumptions. Applying Proj^1 when constructing predictions of SAR leads to constrained predictions that are closer to the Fréchet mean than those obtained with Proj^2 . On the other hand, Proj^1 may be less useful for DSAR, as one may obtain $\hat{x}_{n+2} := \exp(\widehat{R}_{n+1})x_{n+1} \approx x_{n+1}$. Therefore Proj^2 appears to be more suitable for DSAR. In the following, we use Proj^1 for SAR and Proj^2 for DSAR.

5. Applications

5.1 Temperature data

Global warming is expected to lead to more heat waves in the summer. It is then of interest to study and model the time series of the bivariate distributions of daily minimum and maximum temperature. Extreme temperatures are associated with increased health and economic risks. The analysis reported here was inspired by Bhatia and Katz (2021). The temperature data we used have been recorded at airport weather stations in the U.S. over the years and are available

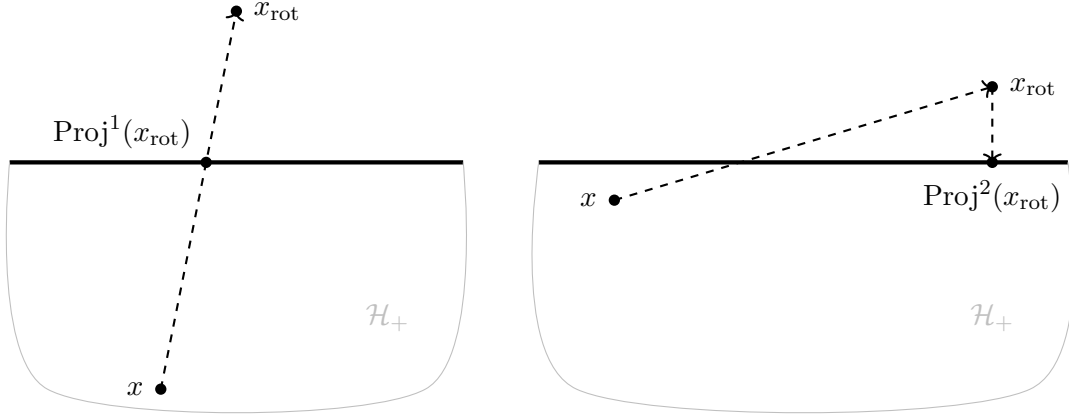


Figure 2: Illustration of the two projection operators Proj^1 and Proj^2 .

at <https://www.ncdc.noaa.gov/cdo-web/search?datasetid=GHCND>.

On the i th day of year $t = 1990, \dots, 2019$, we observe two temperatures $(z_{t,i}, w_{t,i})$, where $z_{t,i}, w_{t,i}$ are minimum and maximum that temperature of each 24 hour period, respectively. We assume that the distribution of $(z_{t,i}, w_{t,i})$ over the summer months in year t has a density f_t such that

$$\{(z_{t,i}, w_{t,i}) : i = 1, 2, \dots, N\} \sim^{i.i.d} f_t, \quad (7)$$

where $N = 122$ as we define the summer days to be June 1 to September 30.

In a preprocessing step we obtained estimates of the bivariate density functions f_t based on samples (7). A quick and fast smoother that adjusts for boundaries is histogram smoothing, which we implemented with histogram bins of size 50 and then applied the R package “fdapace” (Gajardo et al. 2021) for the smoothing step, where the bandwidth are set to be $(\max_i z_{t,i} - \min_i z_{t,i})/5$ and $(\max_i w_{t,i} - \min_i w_{t,i})/5$, then adjusting the results so that the estimated densities integrate to 1. We thus obtained 30 bivariate density functions for the years from 1990 to 2019, some of which are shown as contour plots in the top six panels of Figure 3 and 4 for Los Angeles International Airport (LAX) and John F. Kennedy International Airport (JFK) respectively.

We used the observed density for 2019 to illustrate the predictions obtained with SAR and DSAR using only the data before 2019 to construct the prediction. The predicted densities are shown as contour plots at the bottom of Figure 3 and 4, where we chose the order $p = 5$ for both SAR and DSAR. We conclude from both the contour plots and the Fisher-Rao distances that SAR works better than DSAR for this prediction, which is not surprising as the temperature distributions for JFK show much less year-to-year variation compared to those at LAX. In addition, we plotted the FR distances between the observed and the fitted densities across time in Figure 5. There is no obvious trend, indicating a basic level of stationarity. Interestingly, there is an obvious outlier for LAX for 2012, a year with the highest temperature on record (113 °F) since 1921.

5.2 Energy data

Data on the sources of energy expressed as fractions or percentages for electricity generation across the entire U.S. are available at <https://www.eia.gov/electricity/data/state/> and constitute a compositional time series. For our analysis we consider three energy sources: (i) Coal or Petroleum; (ii) Natural gas; (iii) Nuclear and Renewables. Sources (i) are known to produce the highest amounts of CO₂ and health damaging air pollutants per Watt generated, while sources (ii) are cleaner but still produce sizeable amounts of CO₂. Sources (iii) do not produce damaging gases while used for energy production but may have some residual risks such as nuclear energy production. Here we consider the compositional time series consisting of the annual proportions of energy generated from sources (i)-(iii), which thus has three components.

The data are available for the years $t = 2005, 2006, \dots, 2019$ and we denote the resulting time series by (U_t, V_t, W_t) , where $U_t, V_t, W_t \geq 0$ and $U_t + V_t + W_t = 1$ for all t . We then obtain the spherical time series $x_t = (\sqrt{U_t}, \sqrt{V_t}, \sqrt{W_t}) \in \mathcal{S}^2$. The data $\{x_t\}_{t=2005}^{2018}$ are used as training set to fit SAR and DSAR models and we aim to predict the proportions of the energy sources for the year 2019. The observed compositions from 2005 to 2018 and the observed, fitted and predicted compositions for 2019 are shown in Figure 6 and illustrated with two types of graphical representations for compositional data. A ternary plot is in the top panel and spherical plot

Los Angeles International Airport

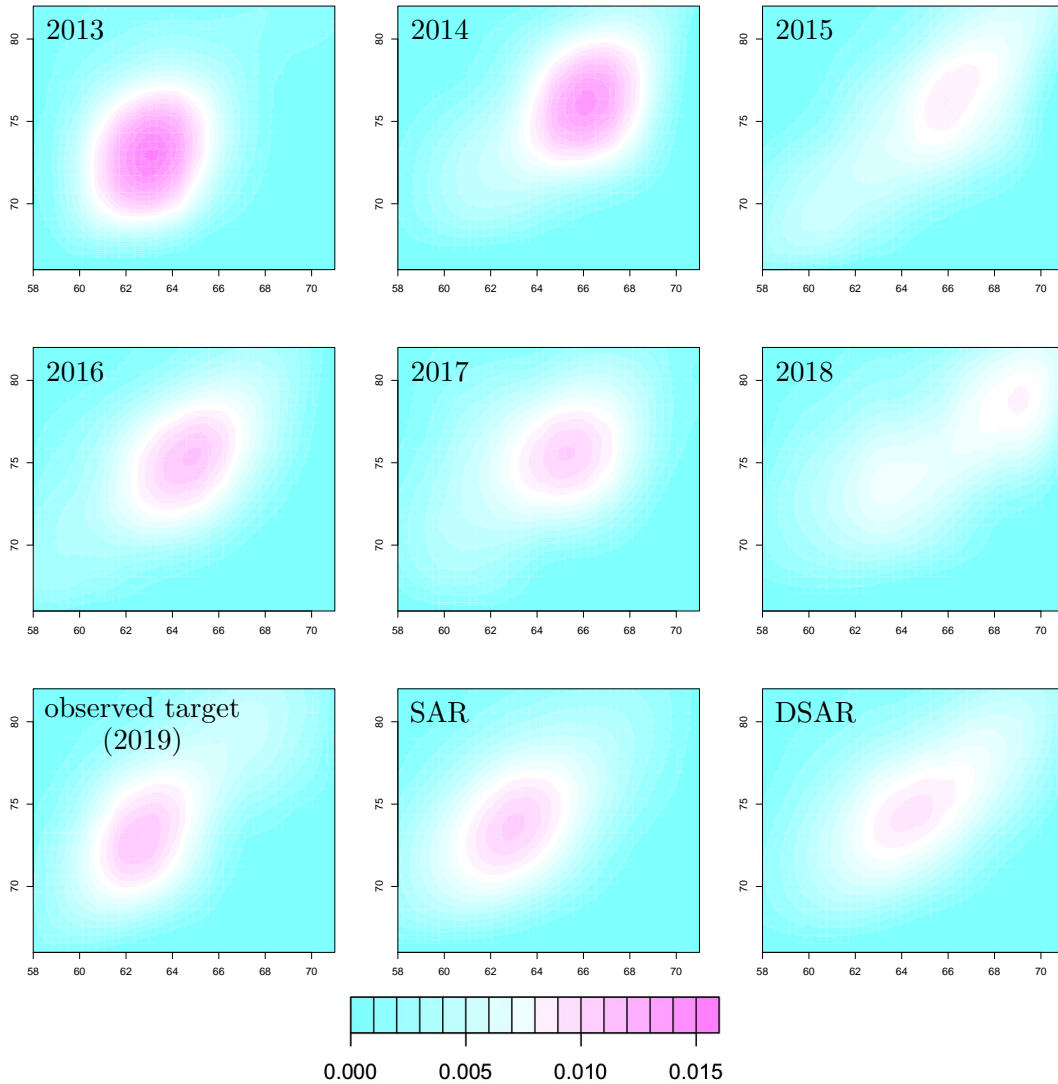


Figure 3: Contour plots of observed and predicted two-dimensional density functions for the distributional time series of temperatures as recorded at LAX. The top six panels show the observed density functions in the training set. The bottom left panels show the observed distribution for 2019 (left); the predicted density using SAR (middle), with Fisher-Rao distance between predicted and observed of 0.197; and the predicted density using DSAR, with Fisher-Rao distance 0.236.

JFK International Airport

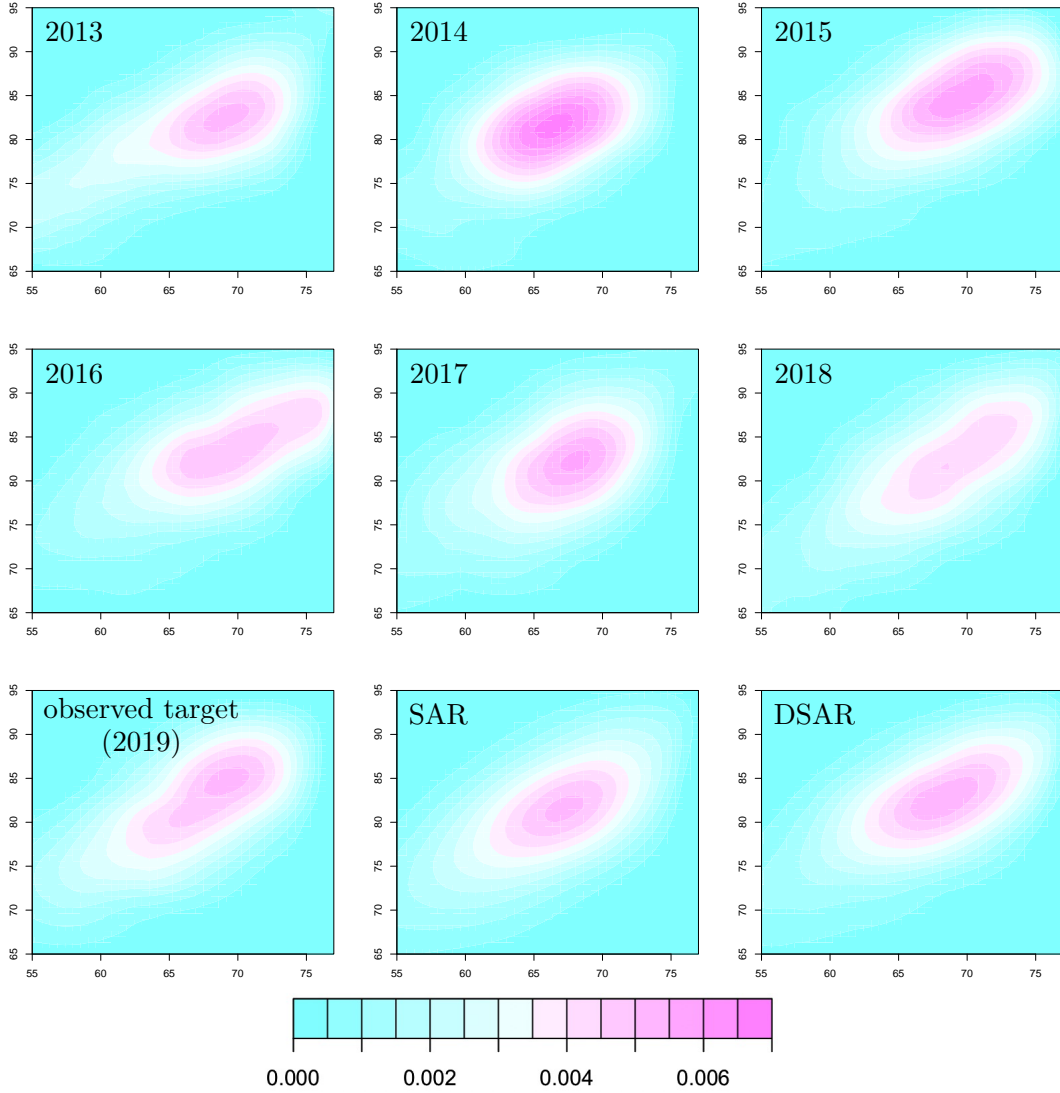


Figure 4: Contour plots of observed and predicted two-dimensional density functions for the distributional time series of temperatures as recorded at JFK. The top six panels show the observed density functions in the training set. The bottom left panels show the observed distribution for 2019 (left); the predicted density using SAR (middle), with Fisher-Rao distance between predicted and observed of 0.147; and the predicted density using DSAR, with Fisher-Rao distance 0.186.

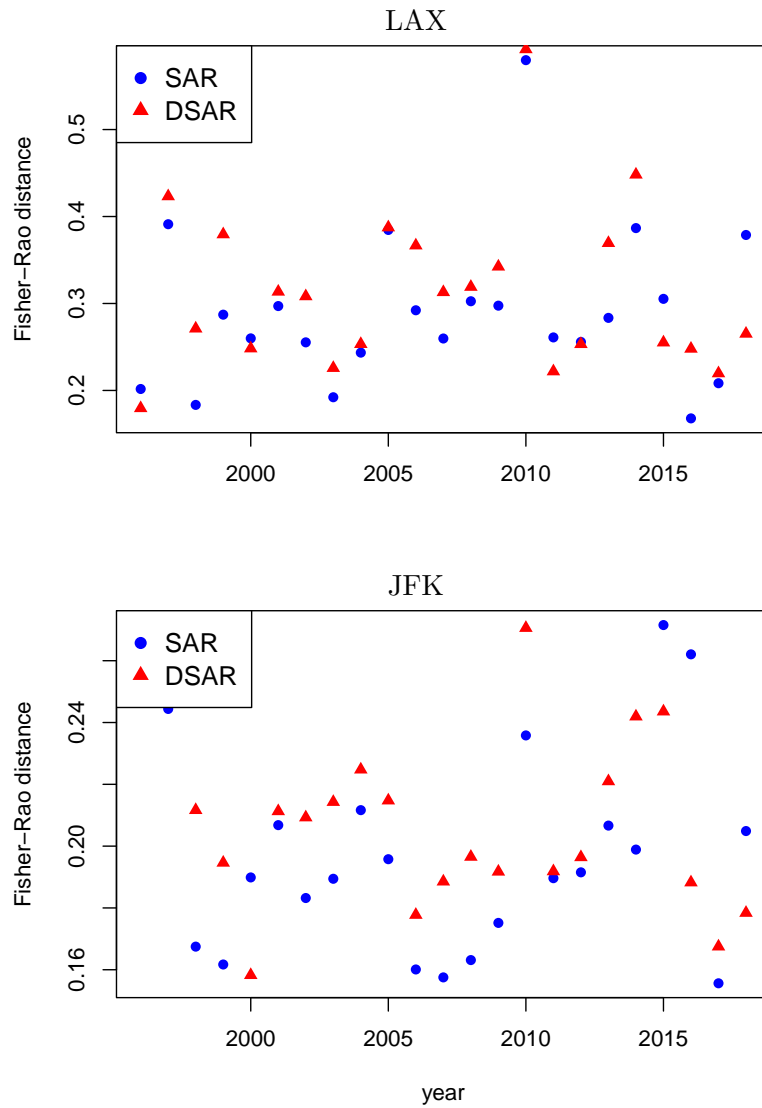


Figure 5: Fisher-Rao distances between observed and fitted densities for each year for distributional time series of two-dimensional temperature distributions.

in the bottom panel, where for the latter we plotted the longitude and latitude of each point $x_t \in \mathcal{S}^2$.

Both plots show a strong trend over the years and the ternary plot indicates that the proportion of energy generated from source (iii) is continuously increasing each year. Correspondingly, the proportion of energy from coal or petroleum is continuously decreasing. The trend indicates some degree of non-stationarity of x_t , while no trend seems to be present when considering the annual increments that correspond to the spherical rotations from one year to the next. It thus appears that the differences $\{x_{t+1} \ominus x_t\}$ are sufficiently stationary. Consequently, we applied model DSAR, for order $p = 2$. Figure 6 indicates that DSAR not only fits the observed data quite well but also produces a reasonable prediction for the energy mix in the year 2019.

6. Discussion

While both compositional and distributional time series can be represented as spherical time series, such time series also arise for directional data (Mardia 2014). Vector time series may also be represented with a spherical component if one is primarily interested in the directions of the vectors over time and less in their length, via polar coordinates. All of this adds to the motivation to study spherical time series, while at the same time, there is little methodology available at this time. In this paper we attempt to address this dearth of methodology by developing an autoregressive modeling approach. We propose to represent rotation operators on spheres by skew-symmetric operators that can be viewed as elements of a Hilbert space so that linear operations become available. Other approaches may also be possible but they have not yet been developed. Our goal is to provide a first modeling approach for this situation as a baseline with which future approaches can be compared.

It is of course possible to use different metrics for both compositional and distributional time series. For compositional data, a classical alternative is the Aitchison geometry (Aitchison 1986), which also has been extended to distributional data (Hron et al. 2016). However, in applications to compositional data this approach does not work if some of the component fractions are zero and then requires arbitrary adjustments, and it also requires the arbitrary selection of a baseline

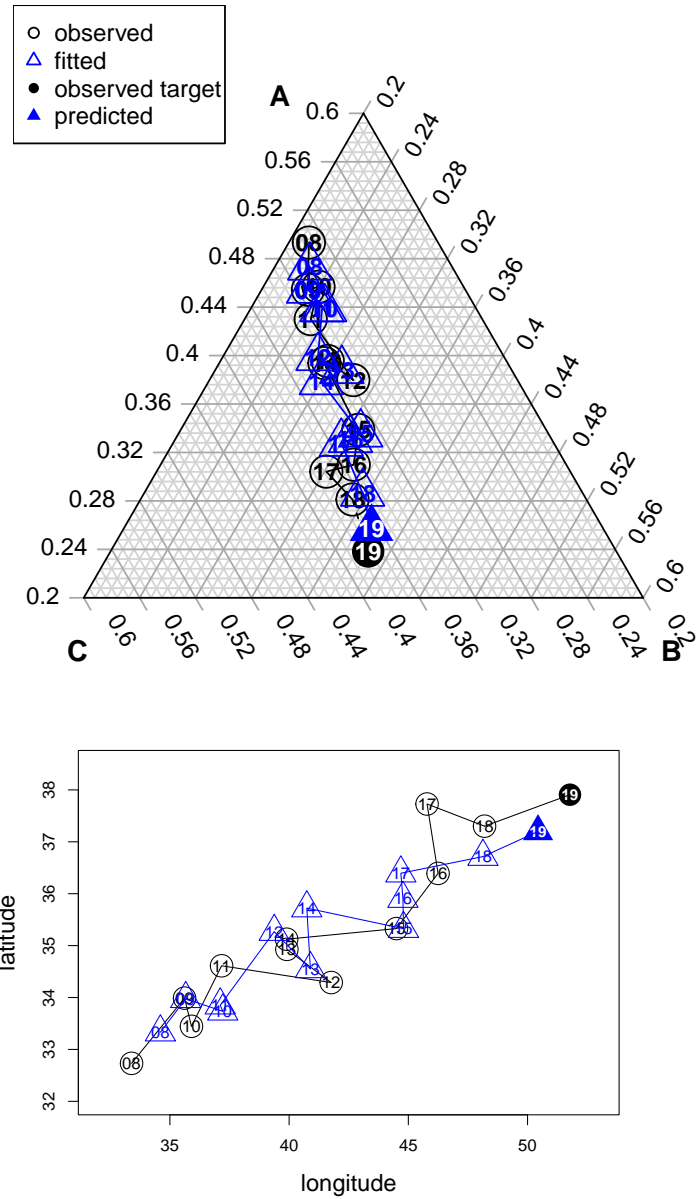


Figure 6: Observed (circles), fitted (triangles) and prediction target (19, circle is observed and triangle is predicted) for the US energy sources compositional time series data, when fitting model DSAR. The numbers 08, \dots , 09, 10, \dots , 19 indicate the years from 2008 to 2019. Top panel: Ternary plot reflecting the compositional nature of the data; here the corner A represents coal or petroleum; B represents natural gas; and C represents nuclear and renewables. Bottom panel: The compositional time series and predictions shown in spherical coordinates. The Fisher-Rao distance between predicted and observed compositions for 2019 is 0.0223.

component; the spherical approach does not face these difficulties (Scealy and Welsh 2014).

For distributional time series an obvious alternative is to consider the space of distributions equipped with the Wasserstein metric (Villani 2003) that is connected with optimal transport. When adopting this metric, the time series is not spherical and needs to be modeled in the Wasserstein manifold, where one can use tangent bundles (Chen et al. 2021; Zhang et al. 2021) or an intrinsic optimal transport approach (Zhu and Müller 2021). However when dealing with the Wasserstein space for multivariate distributions one faces major hurdles in both theory and computation. In contrast the Fisher-Rao metric that we consider here allows seamless extensions to any dimension. When the distributions are unknown, they need to be estimated and density estimation in higher dimensions is subject to the curse of dimensionality. This can be counteracted by assuming that the number of data from which each of the densities is estimated is large.

Further in-depth comparisons of the various possible approaches to distributional and compositional time series will need to await future research. Beyond these two signature applications, autoregressive models for spherical time series provide a useful tool for directional time series and other situations where one has a natural representation of data on a finite- or infinite-dimensional sphere. Another area of future research will be the development of other time series approaches for such data that extend autoregressive models to more complex models for time series such as GARCH models or to the frequency domain.

Finally, the spherical regression models that we have proposed here are also applicable for the case of a multiple regression in a non-time series context, for situations where both predictors and responses are spheres. In this case one has n i.i.d. pairs $(X_{i1}, \dots, X_{im}, Y_i) \in \mathcal{S}$ and aims to model and obtain fits for the regression relation $E(Y|X_1, \dots, X_m)$. To our knowledge, such multiple spherical regression models have not been studied yet.

REFERENCES

Aitchison, J. (1986), *The Statistical Analysis of Compositional Data*, Chapman & Hall, Ltd.

- Bauer, M., Bruveris, M. and Michor, P. W. (2016), ‘Uniqueness of the Fisher–Rao metric on the space of smooth densities’, *Bulletin of the London Mathematical Society* **48**(3), 499–506.
- Bhatia, A. and Katz, J. (2021), ‘Why we are experiencing so many unusually hot summer nights’, *The New York Times* **September 16**, A12.
- Bosq, D. (2000), *Linear Processes in Function Spaces: Theory and Applications*, Springer-Verlag, New York.
- Burago, D., Burago, Y. and Ivanov, S. (2001), *A Course in Metric Geometry*, American Mathematical Society, Providence, RI.
- Chang, T. (1986), ‘Spherical regression’, *Annals of Statistics* **14**(3), 907 – 924.
- Chang, T. (1989), ‘Spherical regression with errors in variables’, *Annals of Statistics* **17**(1), 293 – 306.
- Chen, Y., Lin, Z. and Müller, H.-G. (2021), ‘Wasserstein regression’, *Journal of the American Statistical Association* (xxx), 1–40.
- Dai, X. (2022), ‘Statistical inference on the hilbert sphere with application to random densities’, *Electronic Journal of Statistics* **16**(1), 700–736.
- Dai, X. and Müller, H.-G. (2018), ‘Principal component analysis for functional data on Riemannian manifolds and spheres’, *Annals of Statistics* **46**, 3334–3361.
- Downs, T. D. (2003), ‘Spherical regression’, *Biometrika* **90**(3), 655–668.
- Fan, J. and Yao, Q. (2003), *Nonlinear Time Series: Nonparametric and Parametric Methods*, Springer-Verlag New York.
- Fan, J. and Yao, Q. (2017), *The Elements of Financial Econometrics*, Cambridge University Press.
- Felicísimo, Á. M., Muñoz, J. and González-Solis, J. (2008), ‘Ocean surface winds drive dynamics of transoceanic aerial movements’, *PLoS one* **3**(8), e2928.
- Friedrich, T. (1991), ‘Die Fisher-Information und symplektische Strukturen’, *Mathematische Nachrichten* **153**(1), 273–296.
- Gajardo, A., Carroll, C., Chen, Y., Dai, X., Fan, J., Hadjipantelis, P. Z., Han, K., Ji, H., Müller, H.-G. and Wang, J.-L. (2021), *fdapace: Functional Data Analysis and Empirical Dynamics*.

- R package version 0.5.7, <https://CRAN.R-project.org/package=fdapace>.
- Hron, K., Menafoglio, A., Templ, M., Hruzova, K. and Filzmoser, P. (2016), ‘Simplicial principal component analysis for density functions in bayes spaces’, *Computational Statistics and Data Analysis* **94**, 330–350.
- Kim, P. T. (1998), ‘Deconvolution density estimation on $SO(N)$ ’, *The Annals of Statistics* **26**(3), 1083 – 1102.
- Mardia, K. V. (2014), *Statistics of Directional Data*, Academic Press.
- Martin, M. H. (1932), ‘On infinite orthogonal matrices’, *American Journal of Mathematics* **54**(3), 579–631.
- Marzio, M. D., Panzera, A. and Taylor, C. C. (2019), ‘Nonparametric rotations for sphere-sphere regression’, *Journal of the American Statistical Association* **114**(525), 466–476.
- Müller, H.-G. (2016), ‘Peter Hall, Functional Data Analysis and Random Objects’, *Annals of Statistics* **44**, 1867–1887.
- Pegoraro, M. and Beraha, M. (2021), ‘Projected statistical methods for distributional data on the real line with the wasserstein metric’, *arXiv preprint arXiv:2101.09039* .
- Petersen, A., Liu, X. and Divani, A. A. (2021), ‘Wasserstein f -tests and confidence bands for the fréchet regression of density response curves’, *The Annals of Statistics* **49**(1), 590–611.
- Petersen, A. and Müller, H.-G. (2016), ‘Functional data analysis for density functions by transformation to a Hilbert space’, *Annals of Statistics* **44**(1), 183–218.
- Rosenthal, M., Wu, W., Klassen, E. and Srivastava, A. (2014), ‘Spherical regression models using projective linear transformations’, *Journal of the American Statistical Association* **109**(508), 1615–1624.
- Scealy, J. and Welsh, A. (2011), ‘Regression for compositional data by using distributions defined on the hypersphere’, *Journal of the Royal Statistical Society: Series B (Statistical Methodology)* **73**(3), 351–375.
- Scealy, J. and Welsh, A. (2014), ‘Colours and cocktails: Compositional data analysis’, *Australian & New Zealand Journal of Statistics* **56**(2), 145–169.
- Shi, X., Li, X. and Cai, T. (2021), ‘Spherical regression under mismatch corruption with appli-

cation to automated knowledge translation', *Journal of the American Statistical Association* (xxx), 1–12.

Villani, C. (2003), *Topics in Optimal Transportation*, American Mathematical Society.

Zhang, C., Kokoszka, P. and Petersen, A. (2021), 'Wasserstein autoregressive models for density time series', *Journal of Time Series Analysis* .

Zhu, C. and Müller, H.-G. (2021), 'Autoregressive optimal transport models', *arXiv preprint arXiv:2105.05439* .